

Indirect Optical Control of Microwave Circuits Using Monolithic Optically Variable Capacitors

Amit S. Nagra, *Student Member, IEEE*, Olivier Jerphagnon, Prashant Chavarkar, *Student Member, IEEE*, Michael VanBlaricum, *Senior Member, IEEE*, and Robert A. York, *Member, IEEE*

Abstract— In this paper, we present an integrated circuit technology suitable for low-power bias-free optical control of microwave circuits and antennas. We have integrated miniature photovoltaic arrays with varactor diodes and thin-film resistors to form monolithic optically variable capacitors (OVC's). For the monolithic OVC described here, only 1.5 mW of optical power was required for more than 2:1 change in capacitance (0.9–0.4 pF). Optically controlled microwave circuits such as X-band analog phase shifters and tunable notch filters, which incorporated the monolithic OVC as the control element, were fabricated to demonstrate the potential of this technology.

Index Terms— Optical control, phase shifters, photovoltaic detectors, varactors.

I. INTRODUCTION

CONSIDERABLE attention has been paid to the direct optical control of microwave circuits. Various RF control functions, such as gain control of amplifiers [1]–[3], oscillator frequency tuning and modulation [4]–[7], oscillator injection locking and reference frequency distribution [8], [9], microwave switching, phase shifting, and attenuation [10]–[17] have been demonstrated using direct optical control. In all of the foregoing examples, the microwave devices required external bias, and the optical control signal was injected directly into the device to adjust its microwave performance. For applications such as reconfigurable and frequency agile antennas, active antenna arrays, beam steering grids, etc., metallic bias wires interfere with the radiation patterns. In these situations, it is desirable that the active devices require no external bias and that the control signal be carried into the devices on optical fibers [18]. Optical fibers do not perturb the antenna fields significantly, since they are made of low-permittivity dielectric materials. Indirect optical control is ideal for such applications and bias-free optical control of FET's [19], varactor diodes [18], and p-i-n diodes [20] has been demonstrated.

Indirect optical control relies on a dedicated photovoltaic (PV) detector to convert the optical control signal into an electrical bias signal. The electrical output from the PV detector controls the operating point of the microwave device and,

thereby, the microwave characteristics of the device. Since the optical signal performs both bias and control functions, there is no need for external bias circuitry and bias leads. Another advantage of indirect optical control is that, since the optical detection and microwave functions are separated, the optical and microwave components may be optimized independently of each other. Thus, it is possible to design circuits such that there is no RF penalty for using optical control and, at the same time, make the optical detection process very efficient so that minimum optical powers are required. Previously described work on indirect optical control [18]–[20] relied on commercially available components. These hybrid circuits were large in size, making them unsuitable for embedding in high-frequency circuits and antennas. Also, large-area PV arrays have slow transient response due to large junction capacitance. To address these issues, we decided to monolithically integrate miniature PV arrays with varactor diodes to form optically variable capacitors (OVC's), as proposed by Toyon Research Corporation in [18]. The size of the integrated OVC's is substantially smaller than the corresponding hybrid implementations. The miniature PV arrays have yet another advantage—ease of coupling light into the device. The array size can be matched to the core size of commercially available multimode fibers, thus enabling a simple butt-coupling scheme to illuminate the PV array. Large arrays need beam expanders and additional optics for efficient illumination of the array active area, making the light coupling more difficult and expensive.

This paper describes the design and testing of integrated OVC's that were monolithically fabricated using gallium arsenide (GaAs). The miniaturization of the PV arrays and their integration with the varactor diodes posed some interesting challenges that are addressed here. We have designed, fabricated, and tested microwave circuits that incorporate the OVC's, such as tunable notch filters and phase shifters. The performance of these circuits demonstrates the potential of the proposed monolithic OVC technology for the indirect control of microwave circuits. The circuits needed no external bias and were controlled using low optical powers ($P_{\text{opt}} \leq 1.5$ mW). Also, there was no degradation in microwave performance due to optical control. Preliminary measurements of the transient response of the monolithic OVC were also made, and they indicate that the switching speed of the monolithic OVC is adequate for optical control applications.

II. BASIC PRINCIPLE OF THE OVC'S

The simplified block diagram of the OVC is shown in Fig. 1(a). The OVC is comprised of a PV array that controls

Manuscript received October 1, 1998; revised March 11, 1999. This work was supported by the Office of Naval Research under ONR Young Investigator Award N00014-96-1-0799.

A. S. Nagra, O. Jerphagnon, P. Chavarkar, and R. A. York are with the Electrical and Computer Engineering Department, University of California, Santa Barbara, CA 93106 USA.

M. VanBlaricum is with Toyon Research Corporation, Goleta, CA 93117 USA.

Publisher Item Identifier S 0018-9480(99)05209-6.

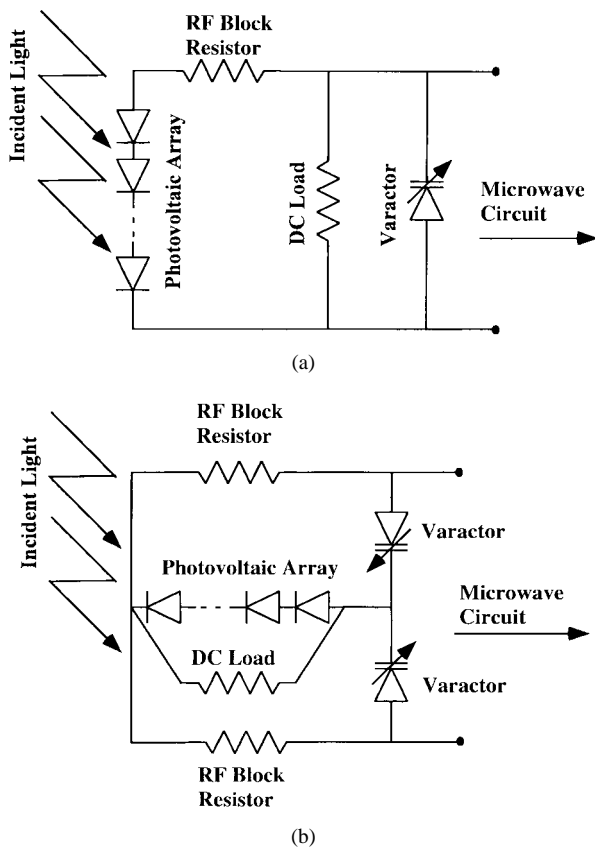


Fig. 1. Circuit schematics for the OVC.

the reverse bias across a varactor diode. A change in the incident optical power leads to a change in the PV array output voltage. This varies the depletion width of the varactor diode and, thereby, its junction capacitance. Hence, this arrangement makes it possible to control the capacitance using optical signals. There are several advantages to this method: 1) the optical signal is used for bias, as well as control of the active device, thus eliminating the need for external bias; 2) since the PV array drives a reverse-biased varactor diode (low leakage current), the optical power requirements are small; and 3) the optical detection and variable capacitance functions are provided by separate components and, hence, it is possible to optimize them independently. The varactor diodes are designed to provide the desired capacitance swing with the lowest possible RF insertion loss, while the PV arrays are designed to provide the desired bias swing across the varactors using as low optical power as possible. Thus, this indirect control scheme provides low-power bias-free optical control of microwave varactors.

Fig. 1(a) and (b) shows two possible configurations of the OVC. The RF-blocking resistor keeps the PV array out of the microwave signal path and ensures that the microwave network just sees the variable capacitance of the varactor diode. The value of this resistance is chosen to be in the kilo-ohm range, so that it acts like a broad-band RF open. In this particular application, it is possible to use RF-blocking resistors instead of blocking inductors, since the reverse-biased varactor diode draws very little current. Hence, the voltage drop across the RF-blocking resistor is negligible and

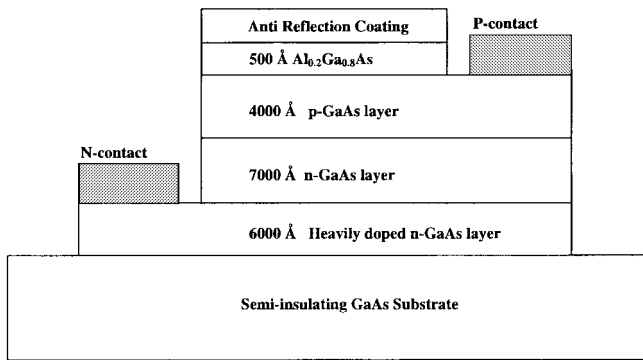
the voltage across the varactor is basically the same as the output voltage from the PV array. Also, blocking resistors are easier to fabricate monolithically and are more compact than inductive chokes. The other component common to both configurations is the fixed dc-load resistor. This resistor serves two purposes: 1) it helps to linearize the PV-array output voltage as a function of optical power and 2) it provides a shunt path for current to flow, enabling the varactor to discharge quickly when the light is switched off. More details on the role of this resistor and guidelines for choosing its value are discussed in later sections.

The configuration shown in Fig. 1(a) is well suited for applications using several devices in series, since the photovoltage across each OVC is floating (no common ground). For applications where several OVC's are connected in parallel, but it is desirable to have independent bias control over each one, the configuration shown in Fig. 1(b) may be used. The advantage of this configuration is that the dc-bias voltage does not appear across the two microwave terminals due to the back-to-back varactor diode arrangement. Also, the configuration in Fig. 1(b) has higher RF power handling capability and better linearity than the simpler configuration of Fig. 1(a). The improved linearity is due to the fact that the capacitance swing induced by the RF voltage is opposite for the two diodes and cancels each other to first order.

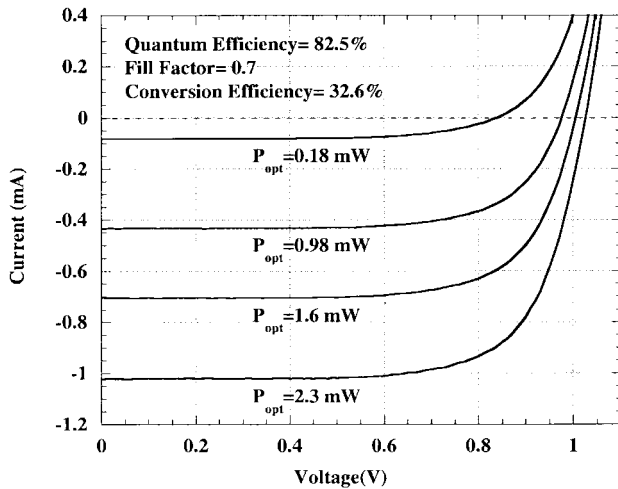
III. MINIATURE PV ARRAYS FOR THE MONOLITHIC OVC'S

The first step in the integration of the monolithic OVC's was the design, fabrication, and testing of miniature PV arrays. As discussed previously, the PV array had to be small, so that the entire OVC could be embedded within a high-frequency antenna/circuit and also because smaller area PV arrays have faster switching times. The GaAs/AlGaAs material system was used for the fabrication of the miniature PV-arrays for several reasons: 1) GaAs-based PV arrays are sensitive to light with wavelength less than 880 nm, hence, relatively inexpensive semiconductor laser diodes/LED's can be used as illumination sources; 2) varactor diodes fabricated on GaAs have higher cutoff frequencies than corresponding silicon-based devices and can be easily integrated with the GaAs PV arrays; 3) semi-insulating GaAs is a good substrate for microwave transmission lines; and 4) GaAs technology is widely used in monolithic-microwave integrated-circuit (MMIC) applications.

There has been a significant amount of research [21]–[23] on GaAs PV cells for terrestrial, as well as space-based, applications. The GaAs-based PV cell used here is essentially a shallow pn junction of the type discussed in [24] with some minor modifications. The differences arise due to the fact that, in our application, the illumination source has a considerably narrow linewidth, as opposed to solar cells that must effectively try and absorb energy over the solar spectrum. Also, due to integration issues, our PV cells are limited to a total thickness of 2 μm , and both the p-contact and n-contact are on the top side of the wafer (back contacts require via holes). Fig. 2(a) shows the details of a single PV cell used here. The topmost layer is the antireflection coating (75 nm of silicon nitride) designed for maximum transmission



(a)

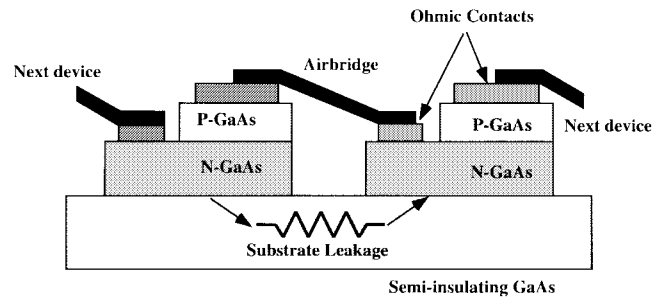


(b)

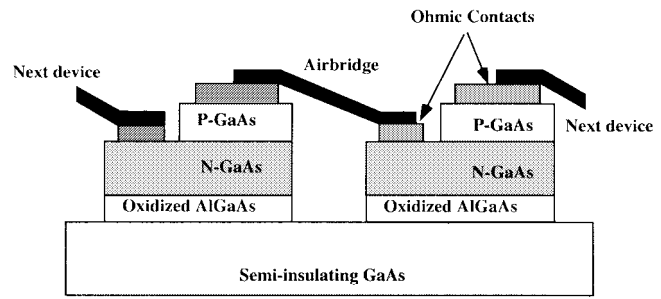
Fig. 2. (a) Epitaxial layer structure of a single GaAs PV cell. (b) $I-V$ curves of a single GaAs PV cell under illumination.

at a wavelength of 630 nm. Below that is an AlGaAs layer (80% Al) that acts as a transparent window for light to pass through. The purpose of this layer is to reduce the surface recombination velocity, so that the carriers generated close to the top of the GaAs layer can diffuse to the pn junction instead of recombining at surface states. The p-type and n-type GaAs layers below that are lightly doped and act as the active layers. The lowest GaAs layer is a heavily doped n-type layer that helps reduce the contact resistance and also provides a back reflection field that reflects minority carriers (holes) toward the junction. Fig. 2(b) shows the performance of a single PV cell under illumination by a diode laser at 630 nm. The external quantum efficiency, which is defined as the ratio of the number of electrical carriers collected at the device terminals to the number of photons incident on the device, was calculated to be 82.5% for the PV cell reported here. The monochromatic energy conversion efficiency of the PV cell is 32.6%, which implies that 32.6% of the incident optical power is made available to the load as electrical power by the PV cell. These values are very reasonable, given the constraints that the device thickness is limited to $2 \mu\text{m}$ and that only top contacts are used for ease of integration (resulting in higher series resistance).

Several (7–10) of the PV cells were connected in series to form PV arrays. Fig. 3 is a schematic of a PV array and shows



(a)



(b)

Fig. 3. Cross section of the PV arrays showing (a) the mesa isolation scheme and (b) the buried oxide isolation scheme.

the pn diodes connected together in series with air bridges. Initially, diodes within the same array were isolated from each other using mesa isolation (active region around each device was etched away down to the semi-insulating substrate). However, the PV arrays generated lower open-circuit voltages than expected under illumination. Careful study [25], [26] of the $I-V$ curves of the illuminated arrays indicated that shunt leakage was the mechanism responsible for the reduced output curves. This shunt leakage was attributed to optically generated carriers in the substrate [see Fig. 3(a)]. Thus, an isolation scheme was required that did not degrade under illumination. Lateral oxidation of AlGaAs has been used for reducing substrate leakage in GaAs HEMT's [27] and we decided to adopt the same technology here. This process involves minimum alteration of the device structure and is easily integrated into our fabrication process. A layer of AlGaAs (98% Al) is incorporated as the bottommost layer [see Fig. 3(b)] and is oxidized thermally in steam [27] to produce a buried oxide layer. This buried oxide layer prevents the photocurrent from leaking into the substrate, and its insulating properties do not degrade under illumination. The $I-V$ characteristics of a seven-cell PV array with and without the buried oxide layer are compared in Fig. 4(a). The illumination source used here is a diode laser operating at 630 nm. Note that, for the PV arrays without the buried oxide, the short-circuit current is the same, but the open-circuit voltages are smaller. Fig. 4(b) shows the measured output voltages of seven-cell PV arrays under open-circuit conditions, and the enhancement in array performance with the buried oxide layer is obvious.

Fig. 5 shows an equivalent circuit model for a PV array, including the effects of the shunt leakage (R_{leakage}) and the fixed dc-load resistor (R_{dc}). This model makes a simplifying assumption that all the diodes are uniformly illuminated, so

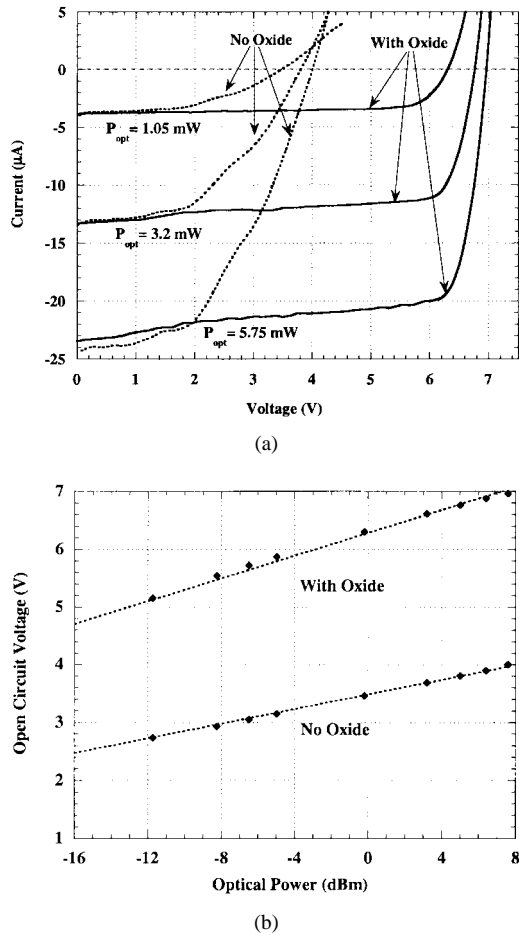


Fig. 4. (a) I - V curves of seven-cell PV arrays with and without the buried oxide isolation. (b) Measured open-circuit voltages of seven-cell PV arrays with and without buried oxide layer.

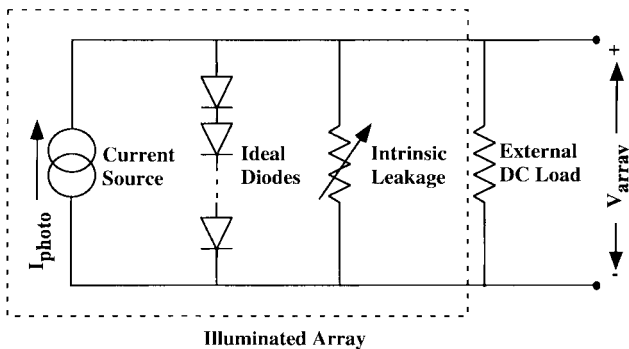


Fig. 5. Equivalent circuit model for a PV array, including leakage effects.

that the same photocurrent I_{photo} is generated in each. The I - V characteristics of this circuit are described by

$$I = I_o(e^{qV/nkT} - 1) - I_{photo} + \frac{V}{R_{dc}} + \frac{V}{R_{leakage}}. \quad (1)$$

Let us examine two extremes.

- 1) When the resistors R_{dc} and $R_{leakage}$ are very large, so that essentially no current flows through them, the output

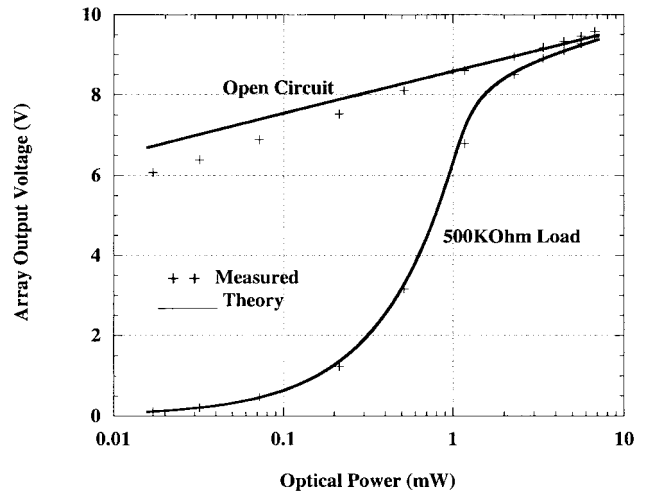


Fig. 6. Comparison of measured and calculated PV-array output voltage.

voltage is given by

$$V = \frac{nkT}{q} \ln \left(\frac{I_{photo}}{I_o} + 1 \right) \quad (2)$$

which is basically the open-circuit voltage [28] generated by an ideal PV array. Since the output voltage follows a logarithmic behavior as indicated in (1), it is very sensitive at low optical powers and not very responsive at higher optical powers.

- 2) When the current in the resistors is larger than the current flowing through the diode (i.e., the resistors are small) the voltage is given by

$$V = I_{photo}(R_{dc} + R_{leakage}). \quad (3)$$

The presence of smaller resistance tends to linearize the response of the array, but, if this resistance becomes too small, then the maximum available output voltage decreases for a given amount of optical power. This is the case when substrate leakage becomes large and explains the lower output voltages seen in arrays without the buried oxide layer.

Fig. 6 is a plot of the measured and calculated response of a ten-cell PV array with buried oxide isolation. For the calculation shown in Fig. 6, the substrate leakage is virtually eliminated due to the use of the buried oxide layer, and so the only shunt resistance is from the fixed dc load. For the open-circuit case (no shunt load), the output voltage varies as the logarithm of the incident optical power and is extremely sensitive for small optical powers. In fact, as can be verified from Fig. 6, the voltage becomes as large as 6 V for just 20 μ W of optical power. When loaded with a fixed 500-K Ω load, the response becomes linear at low optical powers and saturates at higher optical powers. Thus, a shunt load resistance in the range 500 k Ω -1 M Ω is desirable, because it gives greater control over the output voltage without significantly reducing the maximum available open-circuit voltage. Note that using a shunt load resistance smaller than 500 k Ω causes the maximum voltage generated by the PV array to decrease and, hence, is avoided.

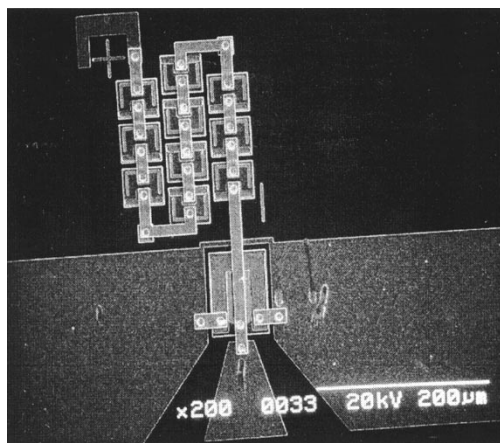
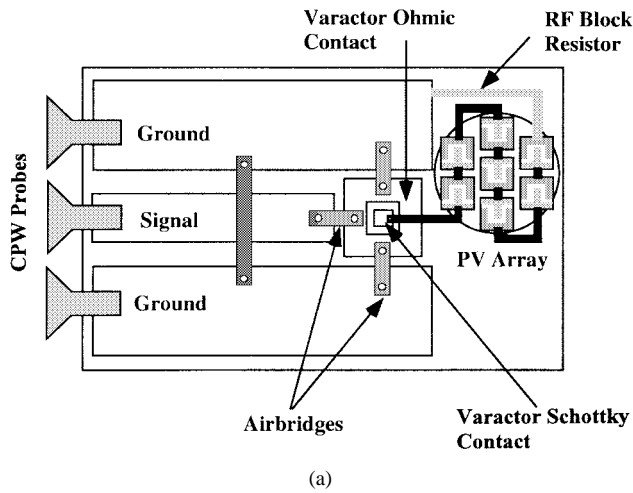


Fig. 7. (a) Schematic showing layout of the integrated OVC. (b) SEM of integrated OVC fabricated on GaAs.

IV. CHARACTERIZATION OF THE OVC AT MICROWAVE FREQUENCIES

The PV array was integrated with a GaAs varactor diode and RF-blocking resistor to complete the monolithic OVC. The varactor diode was fabricated on the same GaAs wafer by etching away the p-type material shown in Fig. 2(a) and placing a Schottky contact (Ti/Pt/Au) on the n-type material. Ohmic contacts (Au/Ge/Ni/Au) were deposited on the heavily doped n-type contact layer and then alloyed at 410 °C for 60 s. A thin NiCr layer (sheet resistance 50 Ω/square) was deposited on the wafer and then patterned to form the RF-blocking resistors. For on-wafer measurements, 1.2-µm-thick gold pads were deposited and all interconnects were made using air bridges. Fig. 7(a) and (b) shows a schematic and SEM, respectively, of the final OVC.

The integrated OVC was placed at the end of a coplanar waveguide (CPW) transmission line structure to perform microwave measurements. Measurements were made on wafer using Cascade Microtech ACP40 probes and an HP 8510 network analyzer. The reflection coefficient (s_{11}) of the OVC was recorded for different illumination intensities. The measured s_{11} was fitted to an equivalent circuit model, and a capacitance value was extracted at 10 GHz. Fig. 8 shows a comparison between the extracted capacitance values and the theoretically

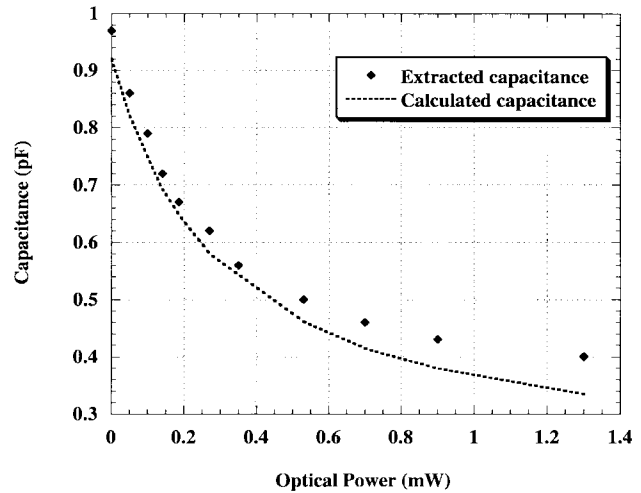


Fig. 8. Comparison of measured and calculated capacitance versus optical power curves for the integrated OVC.

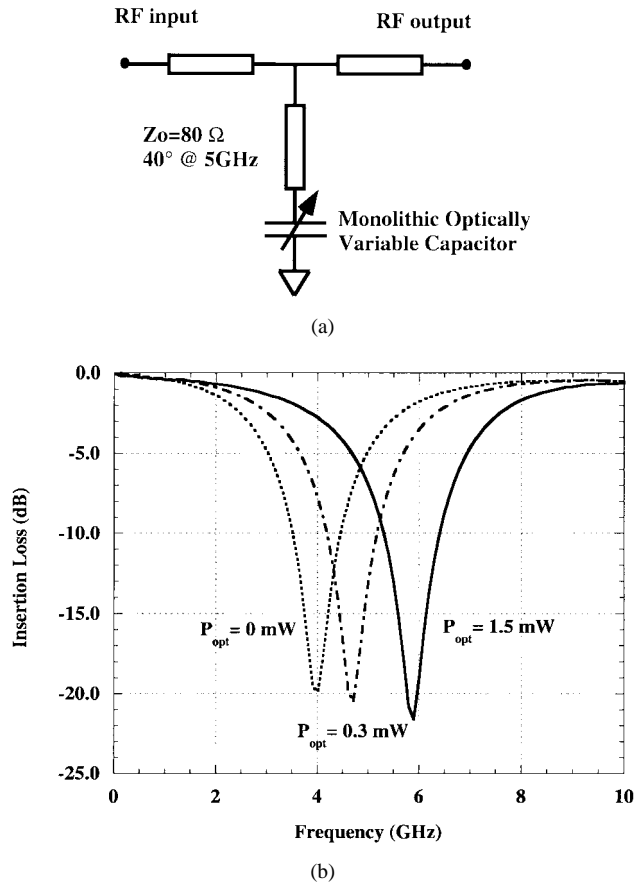


Fig. 9. (a) Equivalent circuit of an optically tunable notch filter incorporating the integrated OVC. (b) Measured performance of an optically tunable notch filter showing 4–5.9-GHz tuning range and greater than 20 dB rejection.

predicted values. The theoretical curve is easily generated by using the expression

$$C = \frac{C_0}{\sqrt{1 - V/V_{bi}}} \tag{4}$$

along with the model (discussed in the previous section) used to predict the array voltage as a function of incident optical power. From the figure, it can be seen that a maximum

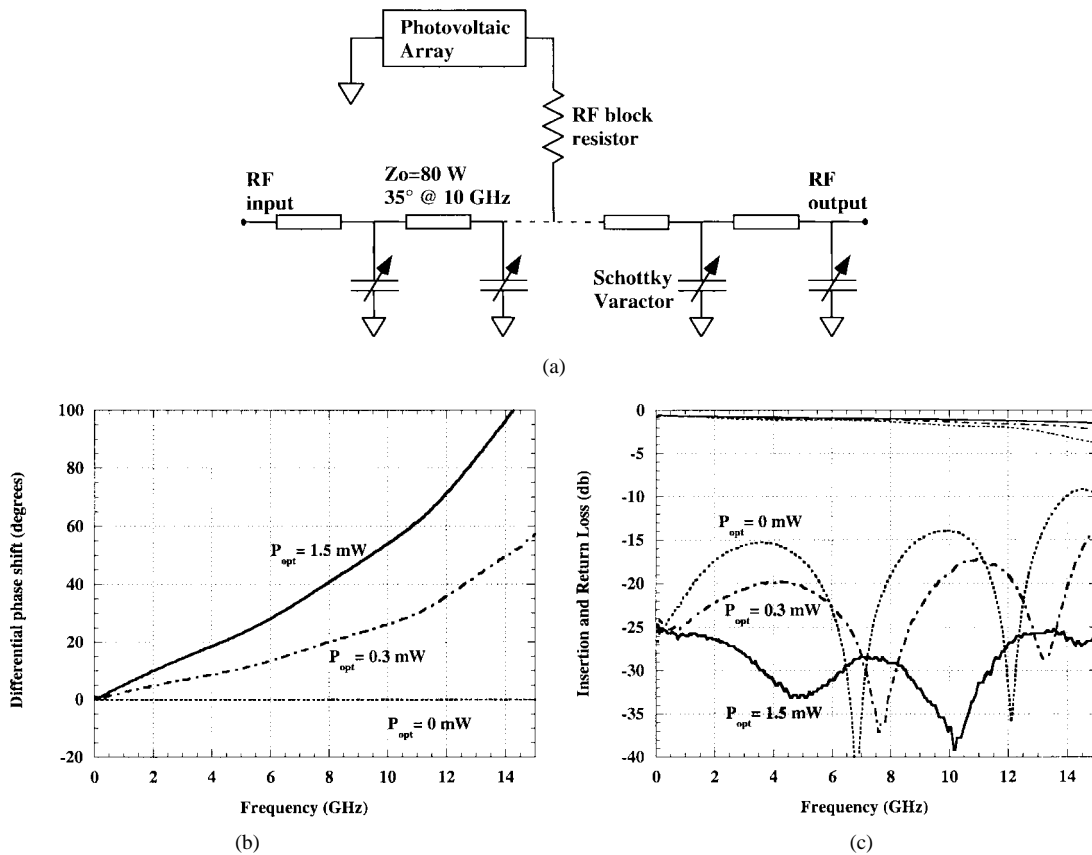


Fig. 10. (a) Equivalent circuit of an optically controlled phase shifter showing a single PV array controlling several varactor diodes. (b) Measured phase shift versus frequency for different optical powers. (c) Insertion and return loss performance of the optically controllable phase shifter.

capacitance variation from 0.95 to 0.4 pF is possible and requires only 1.5 mW of optical power.

We have designed, fabricated, and tested microwave circuits that incorporate the monolithic OVC as the optically controlled element. The circuits were fabricated on the same GaAs wafer as the OVC. Fig. 9(a) shows the schematic of a simple notch filter. It is essentially a single-shunt resonator with the OVC embedded in the resonator to alter the resonance frequency. Under illumination, the PV-array output voltage increases, which, in turn, causes the varactor capacitance to decrease. As a result of lower capacitive loading, the resonance frequency shifts upward, as can be verified from Fig. 9(b), which shows the transmission through this structure for different levels of illumination. The rejection in the stopband is greater than 20 dB, and the tuning range is from 4 GHz (no illumination) to 5.9 GHz (1.5 mW of optical power).

We also fabricated some optically controlled analog phase shifters operating in the X band. The schematic for the phase-shifter circuit is shown in Fig. 10(a). The circuit is comprised of a high-impedance line periodically loaded with varactor diodes. This circuit is similar to nonlinear transmission lines [29] used for pulse compression, shock-wave generation, etc. In the small-signal (linear) regime, the varactor diode loaded transmission line behaves like a synthetic transmission line, the phase velocity of which can be varied by changing the capacitance of the loading varactor diodes. Since all the varactor diodes require the same control signal, only one PV array is required for the circuit. The PV array is connected

in such a way that the array output voltage reverse biases all the varactors by the same amount. The circuit we fabricated was capable of generating a maximum phase shift of 70° at 12 GHz when the optical power was increased from 0 to 1.5 mW. Fig. 10(b) depicts the phase shift as a function of frequency for different optical power levels. The maximum insertion loss for this circuit was 2 dB and the return loss better than 15 dB over all illumination states. The loss performance of this phase shifter (0.028 dB/degree phase shift) is significantly better than the optically controlled Schottky-contacted CPW phase shifters (0.11 dB/degree phase shift) described in [10]. Still better performance is possible by optimization of the phase shifter design, as discussed in [30].

V. TRANSIENT RESPONSE OF THE OVC'S

In order to characterize the transient response of the OVC's, a directly modulated semiconductor laser diode (wavelength 630 nm) was used as the illumination source. The rise and fall times of the light output from the laser diode were measured using a fast photodetector and were estimated to be 200 ns (limited by response of the laser drive circuit). We used SP101 active probes from Lucas Signatone (input resistance $\sim 1 \text{ M}\Omega$, input capacitance 0.1 pF) to sample the PV-array output voltage without loading the circuit. Fig. 11 shows the transient response of a ten-cell PV array (capacitance 0.3 pF) to 630 nm light that was intensity modulated at a frequency of 50 kHz. The rise and fall times for the array output voltage

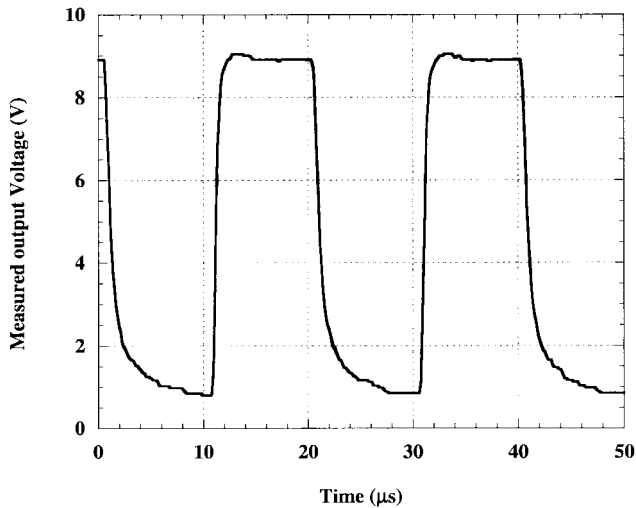


Fig. 11. Transient response of the PV array to intensity modulated light.

were measured to be 0.5 and 1.7 μs , respectively. As discussed in [19] and [31], the rise time is determined by the time it takes the photocurrent to charge up the junction capacitance ($t_r \approx CV/I_{\text{photo}}$). Since the photocurrent scales linearly with incident optical power, higher optical powers result in faster rise times. The fall time on the other hand is independent of optical power and is determined by the time required to discharge the junction capacitance through the dc-load resistor (R_{dc}). Hence, smaller values of the dc-load resistor help speed up the fall time. However, as discussed previously, if this resistor becomes smaller than 500 k Ω , then the maximum PV-array voltage decreases. As a compromise, the value of the shunt load resistor is chosen to be 1 M Ω . Both the rise and fall times decrease with a decrease in the total capacitance, and so, going to smaller PV arrays ensures faster transient response. The smaller junction capacitance of the miniature GaAs PV arrays is the reason why the transient times reported here are faster than those in [19].

VI. CONCLUSIONS

We have integrated miniature PV arrays with varactor diodes and passive components to form monolithic OVC's. We have designed, fabricated, and tested microwave circuits that incorporate the monolithic OVC as a control element. An optically tunable notch filter (>20 dB rejection) with 4–5.9 GHz tuning range and an optically controlled phase shifter with 0°–70° phase shift (insertion loss <2 dB) were demonstrated. These circuits required a maximum optical power of only 1.5 mW and did not need any external dc bias. We also presented the transient response of the integrated OVC's, which showed improvement over earlier hybrid versions. In summary, we have demonstrated that the monolithic OVC is suitable for indirect optical control of microwave circuits and requires low optical powers.

ACKNOWLEDGMENT

The authors would like to acknowledge Prof. U. K. Mishra and his research group at the University of California at

Santa Barbara, for valuable discussions regarding the lateral oxidation of buried AlGaAs layers.

REFERENCES

- [1] A. A. De Salles and J. R. Forrest, "Theory and experiment for the GaAs MESFET under optical illumination," in *Proc. 11th European Microwave Conf.*, Amsterdam, The Netherlands, 1981, pp. 280-284.
- [2] A. A. De Salles, "Optical control of GaAs MESFET's," *IEEE Trans. Microwave Theory Tech.*, vol. MTT-31, pp. 812-220, Oct. 1983.
- [3] R. N. Simons, "Microwave performance of an optically controlled AlGaAs/GaAs high electron mobility transistor and GaAs MESFET," *IEEE Trans. Microwave Theory Tech.*, vol. MTT-35, pp. 1444-1455, Dec. 1987.
- [4] A. J. Seeds and A. A. De Salles, "Optical control of microwave semiconductor devices," *IEEE Trans. Microwave Theory Tech.*, vol. 38, pp. 577-585, May 1990.
- [5] J. R. Forrest and A. J. Seeds, "Optical control of IMPATT microwave oscillators," in *Proc. 1978 Int. Electron Devices Meeting*, Washington, DC, 1978, pp. 282-285.
- [6] P. Freeman, Z. Xiangkun, I. Vurgaftman, J. Singh, and P. Bhattacharya, "Optical control of 14 GHz MMIC oscillators based on InAlAs/InGaAs HBT's with monolithically integrated optical waveguides," *IEEE Trans. Electron Devices*, vol. 43, pp. 373-379, Mar. 1996.
- [7] P. R. Herczfeld, A. S. Daryoush, A. Rosen, V. M. Contarino, and P. Stabile, "Optically controlled microwave devices and circuits," *RCA Rev.*, vol. 46, pp. 528-551, Dec. 1985.
- [8] R. D. Esmen, L. Goldberg, and J. F. Weller, "Optical phase control of an optically injection-locked FET microwave oscillator," *IEEE Trans. Microwave Theory Tech.*, vol. 37, pp. 1512-1518, Oct. 1989.
- [9] D. Yang, P. Bhattacharya, R. Lai, T. Brock, and A. Paoella, "Optical control and injection locking of monolithically integrated In_{0.53}Ga_{0.47}AsIn_{0.52}Al_{0.48}As MODFET oscillators," *IEEE Trans. Electron Devices*, vol. 42, pp. 31-37, Jan. 1995.
- [10] P. Cheung, D. P. Neikirk, and T. Itoh, "Optically controlled coplanar waveguide phase shifters," *IEEE Trans. Microwave Theory Tech.*, vol. 38, pp. 586-595, May 1990.
- [11] P. J. Stabile, A. Rosen, and P. R. Herczfeld, "Optically controlled lateral PIN diodes and microwave control circuits," *RCA Rev.*, vol. 47, pp. 443-456, Dec. 1986.
- [12] A. M. E. Safwat, J. Haidar, D. A. M. Khalil, A. Vilcot, M. Bouthinon, H. Elhennawy, and H. F. Ragaie, "An optically controlled microwave matching technique," *Microwave Optical Technol. Lett.*, vol. 11, pp. 284-290, Apr. 1996.
- [13] S. E. Saddow and C. H. Lee, "Optical control of microwave-integrated circuits using high-speed GaAs and Si photoconductive switches," *IEEE Trans. Microwave Theory Tech.*, vol. 43, pp. 2414-2420, Sept. 1995.
- [14] S. E. Saddow, B. J. Thebrez, and C. H. Lee, "An optoelectronic attenuator for the control of microwave circuits," *IEEE Microwave Guided Wave Lett.*, vol. 3, pp. 361-362, Oct. 1993.
- [15] S. J. Rossek and C. E. Free, "Optically controlled microwave switching and phase shifting using GaAs FET's," *IEEE Microwave Guided Wave Lett.*, vol. 5, pp. 81-83, Mar. 1995.
- [16] ———, "Optical control of microwave signals using GaAs FET's," *Electron. Commun. Eng. J.*, vol. 6, pp. 21-30, Feb. 1994.
- [17] R. Kremer, S. Redlich, L. Brings, and D. Jager, "Optically controlled coplanar transmission lines for microwave signal processing," *IEEE Trans. Microwave Theory Tech.*, vol. 43, pp. 2408-2413, Sept. 1995.
- [18] M. L. VanBlaricum, C. J. Swann, and T. L. Larry, "Remote optical control and tuning of antenna elements," in *Proc. URSI Radio Science Meeting*, Newport Beach, CA, 1995, p. 135.
- [19] S. K. Sun, R. Nguyen, C. T. Chang, and D. J. Albares, "Photovoltaic-FET for optoelectronic RF/microwave switching," *IEEE Trans. Microwave Theory Tech.*, vol. 44, pp. 1747-1750, Oct. 1996.
- [20] C. K. Sun, R. Nguyen, D. J. Albares, C. T. Chang, and P. Cunningham, "Photovoltaic-PIN switches for a photonically reconfigurable monopole antenna," in *Proc. Photonic Systems for Antenna Applications Symp.*, Monterey, CA, 1997, pp. 197-199.
- [21] J. C. C. Fan, A. R. Calawa, R. L. Chapman, and G. W. Turner, "Efficient shallow-homojunction GaAs solar cells by molecular beam epitaxy," *Appl. Phys. Lett.*, vol. 35, pp. 804-806, Nov. 1979.
- [22] R. C. Miller, B. Schwartz, L. A. Koszi, and W. R. Wagner, "A high-efficiency GaAlAs double-heterostructure photovoltaic detector," *Appl. Phys. Lett.*, vol. 33, pp. 721-723, Oct. 1978.
- [23] J. M. Woodall and H. J. Hovel, "High-efficiency Ga_{1-x}Al_xAsGaAs solar cells," *Appl. Phys. Lett.*, vol. 21, pp. 379-381, Oct. 1972.
- [24] M. R. Melloch, E. S. Harmon, and K. A. Emery, "Large-area, 8-cm² GaAs solar cells fabricated from MBE material," *IEEE Electron Device Lett.*, vol. 12, pp. 137-139, Mar. 1991.

- [25] A. S. Nagra, P. Chavarkar, C. J. Swann, T. Larry, M. L. VanBlaricum, U. K. Mishra, and R. A. York, "Monolithic optically variable capacitors for tunable microwave antennas," in *Proc. IEEE/Cornell Conf. Advanced Concepts in High Speed Semiconductor Devices and Circuits*, Ithaca, NY, 1997, pp. 69–78.
- [26] A. S. Nagra, M. L. VanBlaricum, and R. A. York, "Low-power indirect optical reactance control using monolithic GaAs OVC technology," in *Proc. Photonic Systems for Antenna Applications Symp.*, Monterey, CA, 1998.
- [27] P. Parikh, P. Chavarkar, and U. Mishra, "First demonstration of GaAs on insulator technology," in *54th Annu. Device Res. Conf. Dig.*, Santa Barbara, CA, 1996.
- [28] H. J. Hovel, *Solar Cells, Semiconductors and Semimetals*, vol. 11. New York: Academic, 1975.
- [29] M. J. W. Rodwell, M. Kamegawa, R. Yu, M. Case, E. Carman, and K. S. Giboney, "GaAs nonlinear transmission lines for picosecond pulse generation and millimeter-wave sampling," *IEEE Trans. Microwave Theory Tech.*, vol. 39, pp. 1194–1204, July 1991.
- [30] A. S. Nagra and R. A. York, "Distributed analog phase shifters with low insertion loss," *IEEE Trans. Microwave Theory Tech.*, submitted for publication.
- [31] A. Madjar, A. Paoletta, and P. R. Herczfeld, "Modeling the optical switching of MESFET's considering the external and internal photo-voltaic effects," *IEEE Trans. Microwave Theory Tech.*, vol. 42, pp. 62–67, Jan. 1994.

Amit S. Nagra (S'92) received the B.E. degree in electrical engineering in 1994 from Regional Engineering College, Tiruchirapalli, India, and the M.S. degree in electrical engineering in 1997 from the University of California, Santa Barbara, where he is currently working towards the Ph.D. degree in electrical and computer engineering.

His research interests include optical control of microwave circuits, microwave photonics, diode-loaded transmission lines, and application of ferroelectric materials to microwave and millimeter-wave circuits and systems.

Olivier Jerphagnon received the Master of Engineering degree from Grenoble Institute of Technology, Grenoble, France, in 1998. He is currently working towards the M.S. degree in electronics and photonics at the University of California, Santa Barbara, as an exchange student from the University of Grenoble, Grenoble, France.

His research interests include high-speed optoelectronics and new generation of optical networks.

Prashant Chavarkar (S'93) was born in Bombay, India, in 1970. He received the B. Tech and M. Tech. degrees in electrical engineering from Indian Institute of Technology, Bombay, India, in 1991 and 1993, respectively. He is currently working towards the Ph.D. degree at the University of California, Santa Barbara.

His research interests include molecular beam epitaxial growth and fabrication of GaAs- and InP-based electronic and optoelectronic devices and device applications of oxides formed by oxidation of AlAs's.

Michael VanBlaricum (S'68–M'76–SM'91) was born in Olney, IL. He received the B.S., M.S., and Ph.D. degrees in electrical engineering from the University of Illinois, Urbana-Champaign, in 1972, 1974, and 1976, respectively.

Since 1989, he has been with Toyon Research Corporation, Santa Barbara, CA, where he is presently a Vice President. He is responsible for research and development studies of advanced antenna and photonic systems with a focus on photonically reconfigurable antenna designs. He created and chaired the DARPA Photonic Systems for Antenna Applications Symposium (PSAA). He is the author of over 60 technical papers and wrote the RCS chapter in *Introduction to Ultrawideband Radar Systems* (Boca Raton, FL: CRC Press).

Dr. VanBlaricum is a member of URSI Commission B, Sigma Xi, Tau Beta Pi, and Eta Kappa Nu.

Robert A. York (S'85–M'89) received the B.S. degree from the University of New Hampshire, Durham, in 1987 and the M.S. and Ph.D. degrees from Cornell University, Ithaca, NY, in 1989 and 1991, respectively, all in electrical engineering.

He is currently an Associate Professor of Electrical and Computer Engineering at the University of California, Santa Barbara (UCSB). His group at UCSB is currently involved with the design and fabrication of novel microwave and millimeter-wave circuits, microwave photonics, high-power microwave and millimeter-wave modules using spatial combining and wide-bandgap semiconductor devices, and application of ferroelectric materials to microwave and millimeter-wave circuits and systems.

Dr. York received the Army Research Office Young Investigator Award in 1993 and the Office of Naval Research Young Investigator Award in 1996.